J Computer-Aided Mater Des (2007) 14:389–402
DOI 10.1007/s10820-007-9050-4

Effect of Elastic Anisotropy and Inhomogeneity on Coring Structure Evolution in Pu-Ga Alloys – Phase-field modeling

S. Y. Hu · M. I. Baskes · M. Stan · J. N. Mitchell · J. X. Zhang · L. Q. Chen

Received: 18 January 2007 / Accepted: 23 January 2007 / Published online: 18 July 2007

Abstract A coring structure in which δ (fcc) grains have Ga-rich cores with Ga-poor shells forms during the ε (bcc) to δ (fcc) phase transformations in Pu-Ga alloys. There are considerable differences between the diffusivities of Ga in ε and δ and a large and anisotropic stress field exists in the coring structure due to the large lattice mismatch between these two phases and strong elastic anisotropy. We developed a phase-field model for simulating the coring structure evolution in three dimensions, taking into account the inhomogeneities of both Ga diffusivity and elastic properties. It is shown that the elastic interactions among different oriented δ grains and diffusive Ga atoms affect Ga diffusion path, the coring structure, and the growth kinetics of the δ phase.

Keywords Phase-field method · Coring structure evolution · ε to δ phase transformations and Pu-Ga Alloys

Introduction

In Pu-Ga alloys, a microstructure, a so called coring structure, consisting of δ (fcc) phase grains with Ga-rich cores and Ga-poor edges is formed during cooling because of the considerable difference of Ga diffusivity in the ε ($\sim 10^{-14}$ to 10^{-11} cm^2 sec^{-1}) and δ (10^{-8} to 10^{-7} cm^2 sec^{-1}) phases. The Ga-poor edge is metastable, and may transform to the extremely brittle α phase [1–4]. Therefore, a microstructure with a homogeneous Ga distribution is desired for stable thermodynamic and mechanical properties. The kinetics of the coring structure

S. Y. Hu (✉) · M. I. Baskes · M. Stan
MST-8, Los Alamos National Laboratory, Los Alamos, NM 78545, USA
e-mail: syhu@lanl.gov

J. N. Mitchell
MST-16, Los Alamos National Laboratory, Los Alamos, NM 78545, USA

J. X. Zhang · L. Q. Chen
Department of Materials Science & Engineering, The Pennsylvania State University, University Park, PA 16802, USA

formation and the homogenization of Ga involve Ga diffusion, grain growth, and external cooling process as well as the elastic interaction between diffusive Ga atoms and internal stresses. The main origin of internal stresses is the inverse Bain distortion during the ε to δ transition. Using the lattice constants of the ε and δ phases [5], the Bain distortion results in about 11 percent contraction along two <100> directions and 26% expansion along the other <100> direction in the bcc structure. This is a very large volume and shape change. Due to the fact that both the ε and δ phases have strong elastic anisotropies, and different elastic properties, it is expected that a large and anisotropic stress field is generated during the phase transformation. In addition, the Ga atom is about 6.8% smaller than the Pu atom. Therefore, the elastic interaction between Ga diffusion and internal stresses might affect the Ga diffusion path and impact the evolution of the coring structure. An understanding of such a kinetic process is of extreme importance to the nuclear weapons community for optimizing the casting process and the materials properties, and for predicting stockpile aging.

The phase-field method, based on a diffuse-interface description, is used primarily for modeling and predicting complex microstructure evolution on a mesoscopic length scale in many important materials processes including solidification, ferroelectric domain formation, martensitic transformation, and precipitation [6–10]. We have developed a phase-field model to study the coring structure evolution in our previous paper [11], where the system was assumed to be elastically homogeneous, ie., the ε and δ phases have the same elastic properties. In the present work, the phase-field model has been extended to an elastically inhomogeneous system. The iteration method [10] was employed to calculate the elastic energy in a solid with general elastic anisotropies and inhomogeneity. Such a model allows one to investigate the effect of the inhomogeneity of Ga diffusivity and elastic properties, the elastic energy generated from the lattice mismatch, the elastic interaction between diffusive Ga and the internal stress, and the effect of cooling rate on the coring structure evolution.

Phase-field Model

Description of microstructure

We consider the microstructure evolution during the transformation from the Pu-Ga solid solution ε phase to the δ phase. The phase diagram of Pu-Ga alloys at the Pu-rich side is shown in Figure 1. The initial microstructure is assumed to consist of randomly distributed nuclei of the δ phase in a single crystal of ε phase at a temperature T_0, which lies in the ε and δ two phase region. We study the microstructure evolution during the cooling from T_0 under a constant cooling rate $\dot{T}$. The equilibrium compositions $c_\varepsilon^{eq}(T)$and $c_\delta^{eq}(T)$ of the ε and δ phases during the cooling process are determined from the phase diagram. We also assume the δ phase forms from the matrix ε phase through the inverse Bain distortion [12], as shown in Figure 2. Thus, the ε and δ phases obey the orientation relationships: $(010)_\varepsilon//(110)_\delta$ and $[001]_\varepsilon//[001]_\delta$, and there are three orientational variants of the δ phase. To describe the microstructure, we employ a composition field $c(\mathbf{r}, t)$ for describing the spatial distribution of solute atom Ga, and three order parameter variables $\eta_i(\mathbf{r}, t)(i = 1, 2, 3)$ for representing the three orientation variants of the δ phase. Here $\mathbf{r} = (x, y, z)$ and t are position and time, respectively. $c(\mathbf{r}, t)$, $\eta_1(\mathbf{r}, t)$, $\eta_2(\mathbf{r}, t)$, and $\eta_3(\mathbf{r}, t)$ have equilibrium values $(c_\delta^{eq}(T), 1, 0, 0)$, $(c_\delta^{eq}(T), 0, 1, 0)$, $(c_\delta^{eq}(T), 0, 0, 1)$in three oriented δ phases, and $(c_\varepsilon^{eq}(T), 0, 0, 0)$ in the ε phase. $c_\delta^{eq}(T)$ and $c_\varepsilon^{eq}(T)$ are the equilibrium compositions of Ga in δ and ε phases at temperature T, respectively.

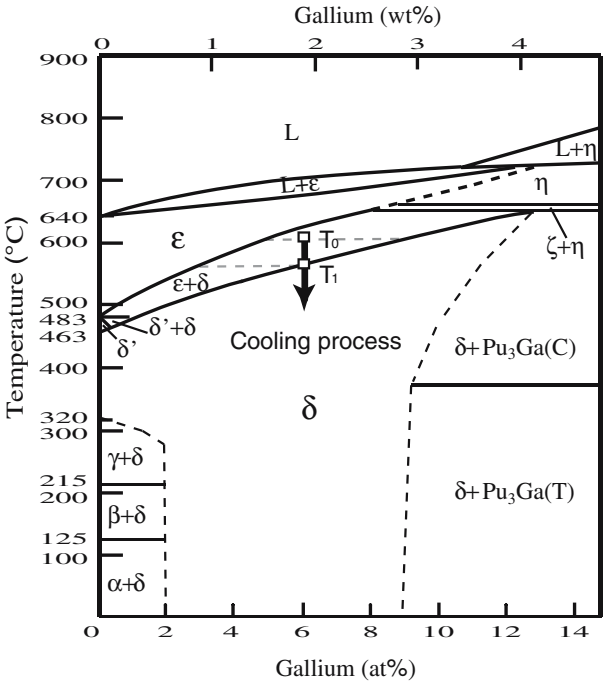

Fig. 1 Phase diagram of Pu-Ga alloys at the Pu rich side generated from the Fig. 2 of Ref. [4].

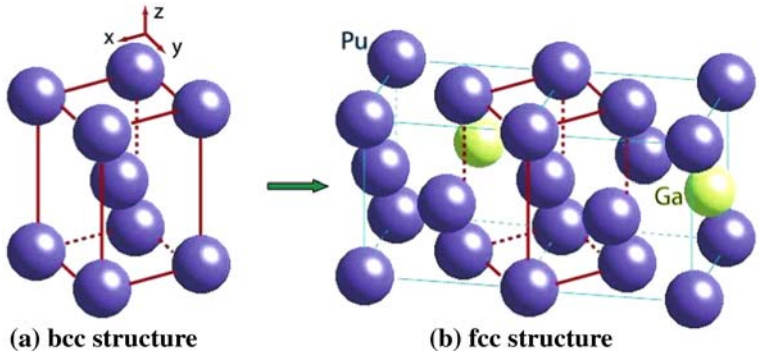

Fig. 2 The inverse Bain distortion from bcc to fcc transformation.

Total free energy of the system

In the phase-field approach framework, the total free energy $F(c, \eta_1, \eta_2, \eta_3, T)$ of the system is described in terms of phase-field variables. The three components of the free energy, chemical free energy, interfacial energy and elastic energy, are represented by the three terms in the following equation:

$$F(c, \eta_1, \eta_2, \eta_3, T) = \int_{V_0} \left[\frac{1}{\Omega_0} G(c, \eta_1, \eta_2, \eta_3, T) + \sum_{i=1}^{3} \frac{\kappa^2}{2} |\nabla \eta_i|^2 + E^{elast} \right] dV \quad (1)$$

where Ω_0 is the molar volume, T is the absolute temperature, κ is the gradient coefficient associated with the interfacial energy, and V_0 is the volume of the system.

The first term in the right side of equation (1) is the chemical free energy. We assume that the material at each point is a mixture of ε and δ phases with the same chemical potential. Then, the chemical free energy per mole of the system $G(c, \eta_1, \eta_2, \eta_3, T)$ can be defined as

$$G(c, \eta_1, \eta_2, \eta_3, T) = (1 - h(\eta_1, \eta_2, \eta_3))\, f^{\varepsilon}(c_{\varepsilon}, T) + h(\eta_1, \eta_2, \eta_3)\, f^{\delta}(c_{\delta}, T) + w g(\eta_1, \eta_2, \eta_3), \tag{2}$$

where $h(\eta_1, \eta_2, \eta_3)$is a shape function, has values of 0 and 1 for the ε and δ phases, respectively, and changes monotonically from 0 to 1 across the interface between the ε and δ phases. $g(\eta_1, \eta_2, \eta_3)$ is a double-well potential, and w is the height of the double well potential. $f^{\varepsilon}(c_{\varepsilon}, T)$ and $f^{\delta}(c_{\delta}, T)$ are chemical free energies per mole of the ε and δ phases, respectively. c_{ε} and c_{δ} are the mole fraction of solute atoms in ε and δ phases, respectively. The mole fractions satisfy the following constraint conditions of mass balance and chemical equilibrium [13],

$$c = [1 - h(\eta_1, \eta_2, \eta_3)]\, c_{\varepsilon} + h(\eta_1, \eta_2, \eta_3)\, c_{\delta}, \quad \frac{\partial f^{\varepsilon}(c_{\varepsilon})}{\partial c_{\varepsilon}} = \frac{\partial f^{\delta}(c_{\delta})}{\partial c_{\delta}}. \tag{3}$$

For simplicity, in the limited Ga concentration interval (0-10%), the chemical free energies $f^{\varepsilon}(c_{\varepsilon}, T)$ and $f^{\delta}(c_{\delta}, T)$ are approximated as parabolic functions:

$$f^{\varepsilon}(c_{\varepsilon}, T) = A_{\varepsilon}(c_{\varepsilon} - c_{\varepsilon}^{eq}(T))^2 \tag{4}$$

and

$$f^{\delta}(c_{\delta}, T) = A_{\delta}(c_{\delta} - c_{\delta}^{eq}(T))^2. \tag{5}$$

The coefficients $A_{\varepsilon}$and A_{δ} are determined by the second derivative of the chemical free energy at the equilibrium composition for ε and δ phases at a given temperature T.

The second term in equation (1) is the interfacial energy. We assume the interfacial energy is isotropic and independent of T, i.e., κ is a constant in the present work. For the case of anisotropic interfacial energy, κ is a function of the interface normal [14].

The third term in equation (1) represents the elastic energy E^{elast} associated with the compositional and structural inhomogeneity. The total stress-free strain $\varepsilon_{ij}^{*}(\mathbf{r})$ related to the lattice mismatch is written as a function of phase-field variables as

$$\varepsilon_{ij}^{*}(\mathbf{r}, t) = \varepsilon_0 \delta_{ij} c(\mathbf{r}, t) + \sum_{k=1,2,3} \varepsilon_{ij}^{*k} \eta_k(\mathbf{r}, t)^2. \tag{6}$$

The first term corresponds to the variation of stress-free lattice parameter, a, with composition. $\varepsilon_0 = \frac{1}{a}\frac{da}{dc}$ is the composition expansion coefficient of the lattice parameter, and δ_{ij} is the Kronecker–Delta function. The strain tensor ε_{ij}^{*k} is related to the lattice mismatch between the matrix ε and k^{th} orientational variant of δ phases. The ε_0 and ε_{ij}^{*k} are determined by the lattice constants and the lattice mismatch between the ε and δ phases [5]. We use $\varepsilon_0 = -0.02$, where the negative sign show that the solute atom Ga is smaller than the host atom Pu. The strain tensor ε_{ij}^{*k} is given

$$\left(\varepsilon_{ij}^{*k}\right) = \begin{pmatrix} -0.098 & 0 & 0 \\ 0 & -0.098 & 0 \\ 0 & 0 & 0.275 \end{pmatrix} \tag{7}$$

for one of the three oriented variants of δ phases with an orientation relationship $(010)_\varepsilon // (110)_\delta$ and $[001]_\varepsilon // [001]_\delta$. Exchanging the strain component ε_{11}^{*k} and ε_{22}^{*k} with ε_{33}^{*k}, respectively, we get the other two strain tensors ε_{ij}^{*k}.

The ε and δ phases have very different elastic properties. At room temperature, the elastic stiffness tensor (GPa) of the δ phase is [15]

$$C_{ij}^{\delta} = \begin{pmatrix} 36 & 26 & 26 & 0 & 0 & 0 \\ 26 & 36 & 26 & 0 & 0 & 0 \\ 26 & 26 & 36 & 0 & 0 & 0 \\ 0 & 0 & 0 & 33 & 0 & 0 \\ 0 & 0 & 0 & 0 & 33 & 0 \\ 0 & 0 & 0 & 0 & 0 & 33 \end{pmatrix} \tag{8}$$

The elastic anisotropic parameter $\varsigma = 2C_{44}^{\delta}/(C_{11}^{\delta} - C_{12}^{\delta})$is about 6.6. For the ε phase, the elastic stiffness tensor is obtained by molecular dynamics simulation at 600 K with the Pu-Ga MEAM potential described in Reference [16],

$$C_{ij}^{\varepsilon} = \begin{pmatrix} 45 & 19 & 19 & 0 & 0 & 0 \\ 19 & 45 & 19 & 0 & 0 & 0 \\ 19 & 19 & 45 & 0 & 0 & 0 \\ 0 & 0 & 0 & 57 & 0 & 0 \\ 0 & 0 & 0 & 0 & 57 & 0 \\ 0 & 0 & 0 & 0 & 0 & 57 \end{pmatrix} \tag{9}$$

The elastic anisotropic parameter $\varsigma = 2C_{44}^{\varepsilon}/(C_{11}^{\varepsilon} - C_{12}^{\varepsilon})$is about 3.5. According to the orientation relationship between the ε and δ phases, when the coordinate system is chosen along the <100> crystalline directions of the ε phase the elastic stiffness tensor of different δ variants $C_{ij}^{\delta k}$ can be obtained by a coordinate transformation where k represents the k^{th} δ variant. For instance, the δ variant denoted by $\eta_1(r, t)$with an orientation relationship $(010)_\varepsilon // (110)_\delta$ and $[001]_\varepsilon // [001]_\delta$has the elastic stiffness tensor:

$$C_{ij}^{\delta 1} = \begin{pmatrix} 64 & 0 & 19.5 & 0 & 0 & 0 \\ 0 & 64 & 26 & 0 & 0 & 0 \\ 19.5 & 26 & 36 & 0 & 0 & 0 \\ 0 & 0 & 0 & 33 & 0 & 0 \\ 0 & 0 & 0 & 0 & 33 & 0 \\ 0 & 0 & 0 & 0 & 0 & 5 \end{pmatrix} \tag{10}$$

Therefore, the elastic energy calculation in the ε to δ phase transformation involves both elastical inhomogeneity and anisotropy. Here, we use the iteration method to calculate the elastic energy. We assume that the local elastic modulus tensor can be presented in terms of the composition field in a linear form,

$$C_{ij}(\mathbf{r}, \mathrm{t}) = C_{ij}^{\varepsilon} + \sum_{k=1,2,3} (C_{ij}^{\delta k} - C_{ij}^{\varepsilon})\eta_k(r, t) \tag{11}$$

The elastic energy is given by

$$E^{elast} = \frac{1}{2} \int \lambda_{ijkl} \varepsilon_{ij}^{el} \varepsilon_{kl}^{el} dV \tag{12}$$

where λ_{ijkl} is the elastic stiffness tensor related to the elastic stiffness tensor C_{ij}, and the elastic strains $\varepsilon_{ij}^{el}(\mathbf{r})$ are the difference between the total strain $\varepsilon_{ij}(\mathbf{r})$ and stress-free strain $\varepsilon_{ij}^{*}(\mathbf{r})$,

$$\varepsilon_{ij}^{el}(\mathbf{r}) = \varepsilon_{ij}(\mathbf{r}) - \varepsilon_{ij}^{*}(\mathbf{r}) \tag{13}$$

We can divide the total strain $\varepsilon_{ij}(\mathbf{r})$ as the sum of homogeneous and heterogeneous strains:

$$\varepsilon_{ij}(\mathbf{r}) = \overline{\varepsilon}_{ij} + \delta\varepsilon_{ij}(\mathbf{r}) \tag{14}$$

where the homogeneous strain $\overline{\varepsilon}_{ij}$ is defined so that $\int \delta\varepsilon_{ij}(\mathbf{r}, \mathbf{t})\, dV = 0$. The homogeneous strain represents the macroscopic shape and volume change, and its magnitude is determined by the boundary condition.

Let us use $u_i(\mathbf{r})$ to denote the i^{th} component of displacement associated with the heterogeneous strain. According to the relationship between strain and displacement, the heterogeneous strain can be expressed as,

$$\delta\varepsilon_{kl} = \frac{1}{2}\left[\frac{\partial u_k}{\partial r_l} + \frac{\partial u_l}{\partial r_k}\right] \tag{15}$$

where r_i is the i^{th} component of the position vector $\mathbf{r}$. The mechanical equilibrium condition requires that

$$\frac{\partial \sigma_{ij}^{el}}{\partial r_j} = 0 \tag{16}$$

where σ_{ij}^{el} are the stress components and are given by

$$\sigma_{ij}^{el}(\mathbf{r}) = \lambda_{ijkl}[\delta\varepsilon_{kl}(\mathbf{r}) + \bar{\varepsilon}_{kl} - \varepsilon_{kl}^{*}(\mathbf{r})] \tag{17}$$

Substituting equations (15) and (17) into equation (16), we obtain

$$\frac{\partial}{\partial r_j}\lambda_{ijkl}\frac{\partial u_k}{\partial r_l} = -\frac{\partial}{\partial r_j}\lambda_{ijkl}[\bar{\varepsilon}_{kl} - \varepsilon_{kl}^{*}(r)] \tag{18}$$

Following the iteration method described in Ref [10] by using the Green functions in elastic anistropic materials [17], we can get the displacement field $u_i(\mathbf{r})$ and the elastic strain. The elastic energy can be calculated by Eq. (12).

Evolution equations

The temporal evolution of the solute composition $c(\mathbf{r}, t)$ and the order parameters $\eta_i(\mathbf{r}, t)$ is described by the Cahn-Hilliard equation [18] and the time-dependent Ginzburg-Landau equation [19]

$$\frac{\partial c}{\partial t} = \nabla \cdot \left(\frac{D(\eta_1, \eta_{2,}\eta_3, T)}{G_{cc}}\nabla\left(\frac{\partial f^{\varepsilon}(c_\varepsilon, T)}{\partial c_\varepsilon} + \frac{\partial E^{elast}}{\partial c}\right)\right), \tag{19}$$

$$\frac{\partial \eta_i}{\partial t} = \frac{L}{\Omega_0}\left[-\frac{\partial G}{\partial \eta_i} - \Omega_0\frac{\partial}{\partial \eta_i}\left(\frac{\kappa^2}{2}|\nabla\eta_i|^2\right) - \Omega_0\frac{\partial E^{elast}}{\partial \eta_i}\right], \tag{20}$$

and the constraint conditions (3). Here, $D(\eta_1, \eta_2, \eta_3, T)$ is the diffusivity of Ga. G_{cc} is the second derivative of G with respect to the composition $c(\mathbf{r}, t)$. And L is a kinetic coefficient related to the interface mobility. For simplicity, the diffusion coefficient is given by

$$D(\eta_1, \eta_2, \eta_3, T) = (1 - h(\eta_1, \eta_2, \eta_3))D_\varepsilon(T) + h(\eta_1, \eta_2, \eta_3)D_\delta(T), \tag{21}$$

where $D_\varepsilon(T)$ and $D_\delta(T)$ are the diffusivity of Ga in the ε and δ phases, respectively. In the previous Pu-Ga alloy diffusion studies [20-21], the diffusivity was expressed in the usual Arrhenius form and fitted by experimental data. Although different investigators reported fairly large difference in the pre-exponential term and the activation energy, all the results showed that the $D_\delta(T)$ is four to seven orders of magnitude smaller than $D_\varepsilon(T)$. We are interested in studying the effect of the Ga diffusivity difference between the ε and δ phases on coring structure evolution. In the calculation below under cooling, the following formula is used to calculate $D_\varepsilon(T)$ and $D_\delta(T)$,

$$\tilde{D}_x(T) = D_x^0 \exp(-Q_x^0/RT), \quad x = \varepsilon, \delta \tag{22}$$

This equation gives $D_\varepsilon(T) = 9.37 \times 10^{-10}[\text{cm}^2/\text{s}]$ to $8.6 \times 10^{-9}[\text{cm}^2/\text{s}]$, and $D_\delta(T) = 5.96 \times 10^{-17}[\text{cm}^2/\text{s}]$ to $3.15 \times 10^{-14}[\text{cm}^2/\text{s}]$ in the temperature range $T = 500$ K to 600 K.

Numerical Method and Input Data

In all simulations, periodic boundary conditions are applied in x-, y- and z-directions. The kinetic equations (19-20) are solved numerically using the Fourier-Spectral method [22]. Based on the phase diagram in Figure 1, we assume that ε and δ coexist at the initial temperature T_0, and the equilibrium compositions vary linearly with the temperature as

$$c_x^{eq}(T) = c_x^{eq}(T_0) + \left[c_x^{eq}(T_0) - c_x^{eq}(T_1)\right] \frac{T - T_0}{T_0 - T_1}, x = \varepsilon \text{ and } \delta. \tag{23}$$

The model and simulation parameters are listed in Table 1. The parameters $\kappa$and w are determined by the interfacial energy σ and interface thickness λ with the relationship,

$$\kappa = \sqrt{\frac{3\sigma\lambda}{\alpha}}, \tag{24}$$

$$w = \frac{6\alpha\sigma\Omega_0}{\lambda}, \tag{25}$$

where α is a constant which depends on the definition of the interface. For example, when the interface is defined in the region between $\eta_i = 0.1$ and $\eta_i = 0.9$, then $\alpha = 2.2$. Furthermore, we assume the phase transition from ε to δ is a diffusion-controlled process. Therefore, a relatively large number L is used in the simulations. The results do not depend on the choice of this number.

Results and Discussion

We focus on studying the effect of the inhomogeneity of Ga diffusivity and elastic energy, and cooling rates on the particle growth. In the simulations, we initially place a spherical fcc nucleus with a radius $R_0 = 5\Delta x$ in a simulation cell $96\Delta x \times 96\Delta x \times 96\Delta x$. The nucleus has the equilibrium composition $c_\delta^{eq}(T_0)$ while the matrix has the composition c_0. First, we study the effect of the inhomogeneity of Ga diffusivity and elastic energy on the particle growth. The simulations are performed at constant temperature T_0. To distinguish these individual effects, we consider three cases: Case1 with homogeneous Ga diffusivity $D = D_\varepsilon = D_\delta = 8.6 \times 10^{-9}[\text{cm}^2/\text{s}]$ and homogeneous elasticity described by equation (8); Case2 with homogeneous Ga diffusivity $D = D_\varepsilon = D_\delta = 8.6 \times 10^{-9}[\text{cm}^2/\text{s}]$ and

Table 1 The model and simulation parameters.

Grid spacing	$\Delta x = 50$nm
Interface thickness	$\lambda = 4\Delta x$
Molar volume	$\Omega_0 = 1.5 \times 10^{-5}$m^3/mol [12]
Interface energy	$\sigma = 0.1$J/m^2
Overall composition	$c_0 = 0.06$
Temperature	$T_0 = 600$K *and* $T_1 = 550$K
Cooling rates	$\dot{T} = 1.8, 2.6,$ and 5.5K/s
A_ε	10^4J/mol
A_δ	10^4J/mol
D_ε^0	5.6×10^{-6}cm^2/s
D_δ^0	1.3cm^2/s
Q_ε^0	55.29kJ/mol
Q_δ^0	156.40kJ/mol
$c_\varepsilon^{eq}(T_0)$	0.05
$c_\varepsilon^{eq}(T_1)$	0.10
$c_\delta^{eq}(T_0)$	0.01
$c_\delta^{eq}(T_1)$	0.05

inhomogeneous elasticity described by equations (8-9); and Case3 with inhomogeneous Ga diffusivity described by equation (22) and inhomogeneous elasticity described by equations (8-9). For three cases, the spherical fcc nucleus has an orientation relationship $(010)_\varepsilon//(110)_\delta$ and $[001]_\varepsilon//[001]_\delta$. Therefore, the lattice mismatch between the ε and δ phases is described by equation (7). Figure 3 presents the particle morphologies for case1 and case 2 at an aging time of 5 seconds. The color bar denotes the Ga concentration. The red interface between the particle and matrix is plotted by the iso-surface of Ga concentration$c = 0.1$. The time evolution of the particle size along $[100]_\varepsilon$, $[111]_\varepsilon$ and $[001]_\varepsilon$ directions is plotted in figure 4 while the time evolution of volume fraction of the δ phase is presented in Figure 5 for the three cases. From these results, we can conclude that (1) the elastic energy associated with the lattice mismatch between the ε and δ phases results in the fastest growth in the $[100]_\varepsilon$ and $[010]_\varepsilon$ directions, and the slowest growth in the $[001]_\varepsilon$ direction, which leads to an elliptical particle. The aspect ratio of the elliptical particle increases with time. (2) The elastic inhomogeneity slows down the growth and increases the aspect ratio of the particle. (3) At constant temperature the effect of the inhomogeneity of Ga diffusivity on the growth is small.

To further understand how the inhomogeneity of Ga diffusivity and elastic energy affect the particle growth, we examine the evolution of Ga composition and internal stress fields. The evolution of the Ga composition profile along a line through the center of the particle in the direction $[100]_\varepsilon$ is plotted in Figure 6 for Case 2 and Case 3. We can see that the Gibbs-Thomson effect causes the equilibrium composition to increase in both the ε and δ phases when the particle is small. As the particle grows, the Gibbs-Thomason effect becomes increasingly less important, and the equilibrium compositions gradually reach the thermodynamic equilibrium compositions which are $c_\delta^{eq}(T_0)$ and $c_\varepsilon^{eq}(T_0)$. The effect of D_δ on the Ga composition profile is that when D_δ is large the extra Ga caused by the Gibbs Thomson effect can quickly diffuse out, leading to a uniform Ga distribution in the fcc particle. However, when D_δ is small the extra Ga cannot diffuse out, which leads to slight Ga segregation. Since the Gibbs Thomson effect only takes place when the particle is small, the effect of D_δ on the

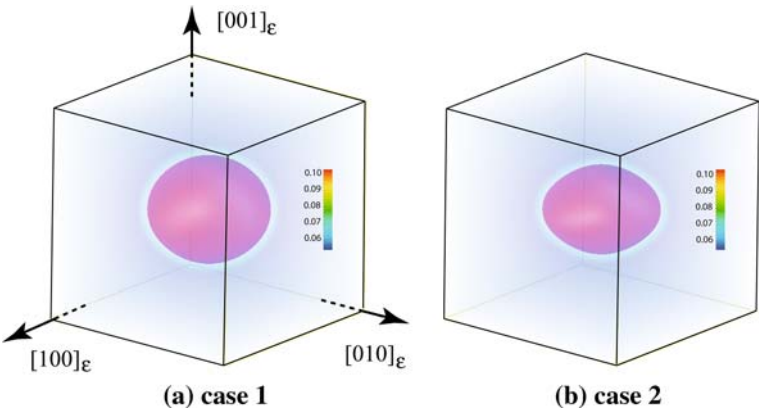

Fig. 3 The morphologies of the δ particles for case 1 and case 2 at an aging time of 5 seconds at T_0 . Color denotes the Ga concentration, and the red surface presents the isosurface with Ga concentration 0.1.

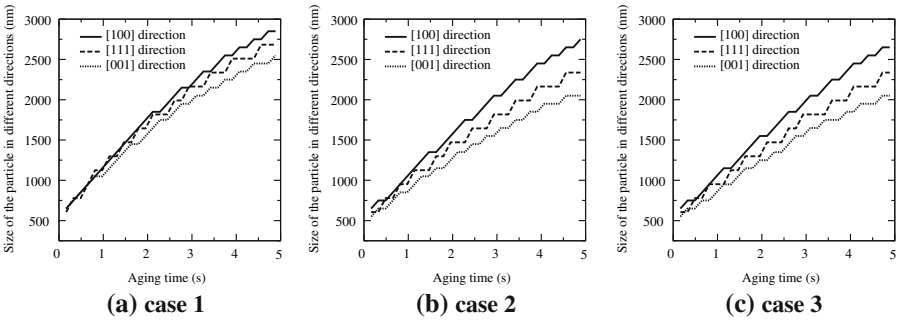

Fig. 4 Particle size along lines through the center of the particle in different directions $[100]_\varepsilon$, $[111]_\varepsilon$ and $[001]_\varepsilon$ as a function of aging time at T_0

Ga segregation and the particle growth kinetics is not important. Of course, this conclusion is only valid for growth under a constant temperature. During cooling, the Ga diffusivity in the fcc phase might affect the growth kinetics because the thermodynamic equilibrium compositions vary with the temperature. A uniform Ga distribution will be reached if the Ga diffusivity in the fcc phase is large enough. Gallium segregation will occur if the Ga diffusivity in the fcc phase is too small. The latter case will cause the formation of the coring structure and affect the growth kinetics of the particle, which can be seen below.

Figure 7a-b shows the evolution of Ga composition and pressure $p = (\sigma_{11} + \sigma_{22} + \sigma_{33})/3$ on the (100) and (110) planes for Case 2. The color presents Ga composition. The white and red lines denote the pressure $p = -0.06$ GPa and $p = 0.06$ GPa, respectively. We can see that the regions circled by the white lines have a compressive stress while the regions circled by the red lines have a tensile stress. Since the Ga atoms have a smaller size than Pu atoms, the elastic interaction should cause Ga atoms to diffuse to the compressive region. As a result, the growth in the $[001]_\varepsilon$ direction is expected to be faster than that in the $[100]_\varepsilon$ and $[010]_\varepsilon$ directions. However, the lattice mismatch between the fcc particle and the bcc matrix in the $[001]_\varepsilon$ direction is much larger than that in the $[100]_\varepsilon$ and $[010]_\varepsilon$ directions. To minimize the elastic energy, the particle prefers to grow in the $[100]_\varepsilon$ and $[010]_\varepsilon$ directions. These results show that the elongation of the particle along the $[100]_\varepsilon$ and $[010]_\varepsilon$ directions

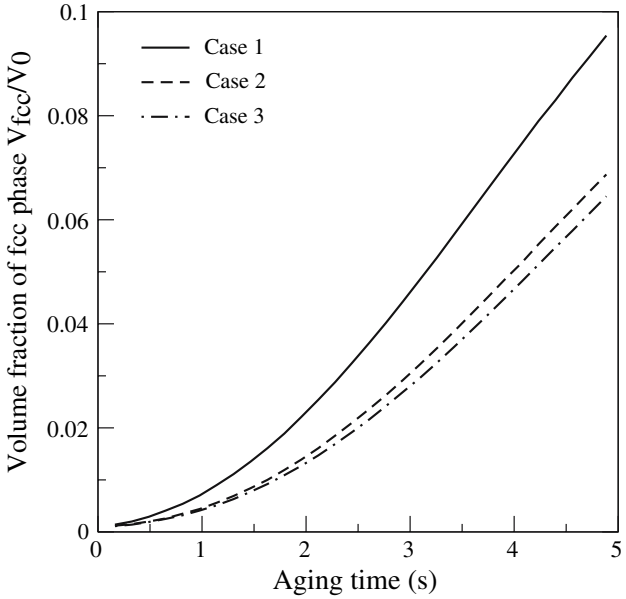

Fig. 5 Volume fraction of the δ particle V_{fcc}/V_0 versus aging time at T_0.

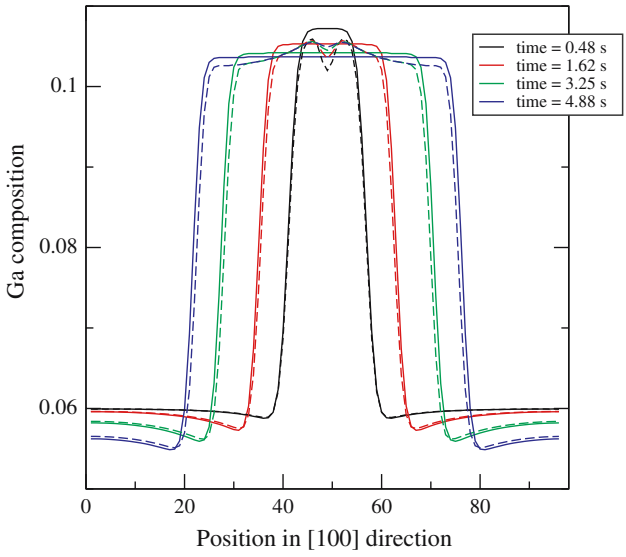

Fig. 6 Evolution of Ga composition profiles along a line in $[100]_\varepsilon$ direction through the center of the particles. Solid lines for Case2 (homogeneous diffusivity $D_\varepsilon = D_\delta = 8.6 \times 10^{-9}\text{cm}^2/\text{s}$) and dashed lines for Case 3 (inhomogenous diffusivity$D_\varepsilon = 8.6 \times 10^{-9}\text{cm}^2/\text{s}$ and $D_\delta = 3.1 \times 10^{-14}\text{cm}^2/\text{s}$).

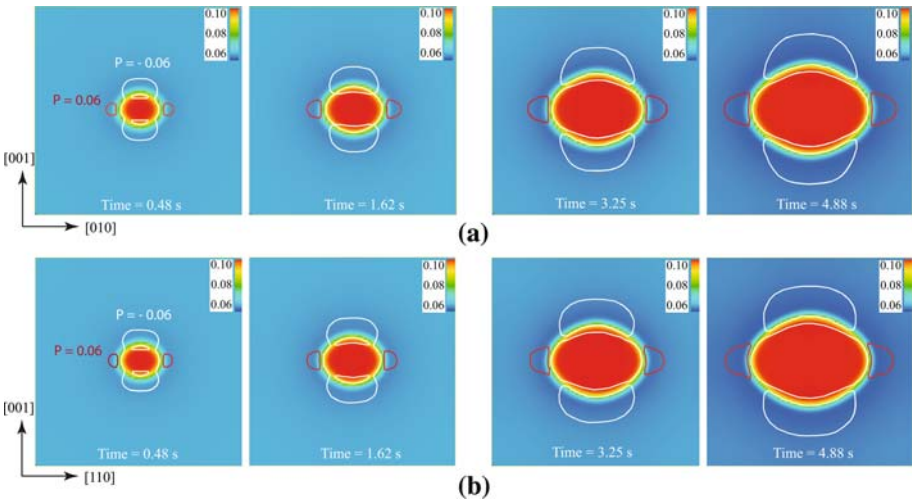

Fig. 7 Evolution of Ga composition and pressure $p = (\sigma_{11} + \sigma_{22} + \sigma_{33})/3$ GPa on (a) the (100) plane and (b) the (110) plane for case 2.

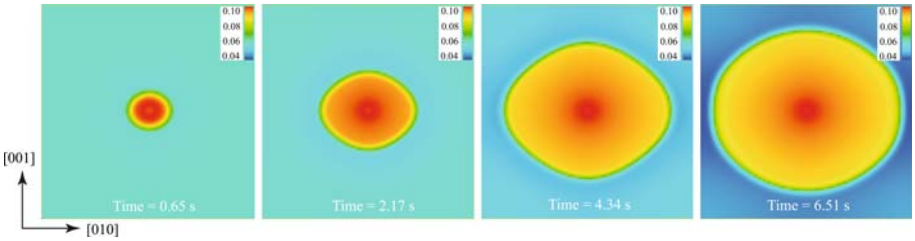

Fig. 8 Evolution of coring structure on (100) plane with a cooling rate 2.6 K/s. The color denotes the Ga composition.

is driven by minimizing the elastic energy while the effect of the Ga diffusion path on the particle elongation is minor.

By adding cooling into the Case 3, we can examine the effect of the cooling rate on the growth of a spherical fcc particle. In the simulations, the temperature decreases with a constant cooling rate from the initial temperature T_0. The thermodynamic equilibrium compositions in the bcc and fcc phases vary with the temperature as described in equation (23). Because of computational limitations, the simulation cell size is limited to $96\Delta x \times 96\Delta x \times 96\Delta x$. The particle grows and fills the whole cell in several seconds. Hence, very large cooling rates $\dot{T} = 1.8, 2.6,$ and 5.5 K/s must be used to capture the effect of cooling rate on the particle growth kinetics. The evolution of Ga composition on the (100) plane is plotted for a cooling rate $\dot{T} = 2.6$ K/s in Fig. 8. The Ga composition profiles along the $[100]_\varepsilon$ and $[001]_\varepsilon$ directions are presented in Figure 9. The composition profile illustrates the coring structure, i.e., the Ga concentration is higher at the center of the particle than at the edge of the particle. Figure 10 shows the effect of cooling rates on Ga composition distributions. It can be seen that the cooling rate significantly affects the Ga segregation inside the fcc particle. The Ga segregation gradually localizes at the center of the particle as the cooling rate increases.
In order to examine quantitatively the Ga segregation in the coring structure, we introduce a coring factor. It is defined as the ratio of the extra Ga in the fcc particle to the overall Ga in the system,

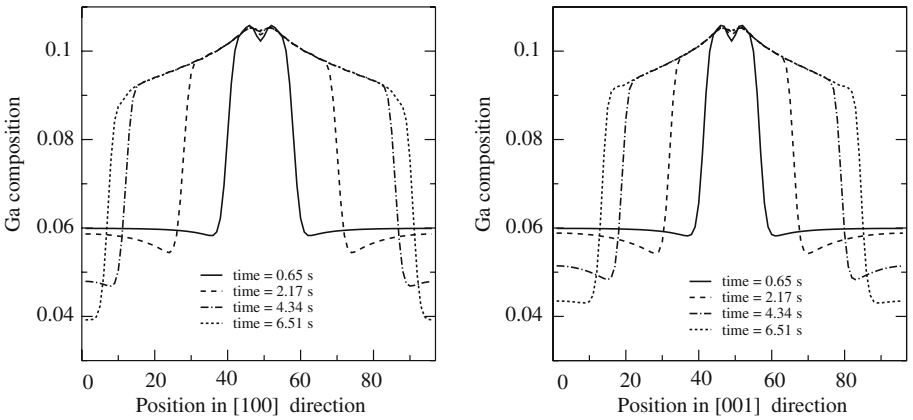

Fig. 9 Evolution of Ga composition with cooling rate 2.6 K/s (a) along the $[100]_\varepsilon$ direction and (b) along the $[001]_\varepsilon$ direction.

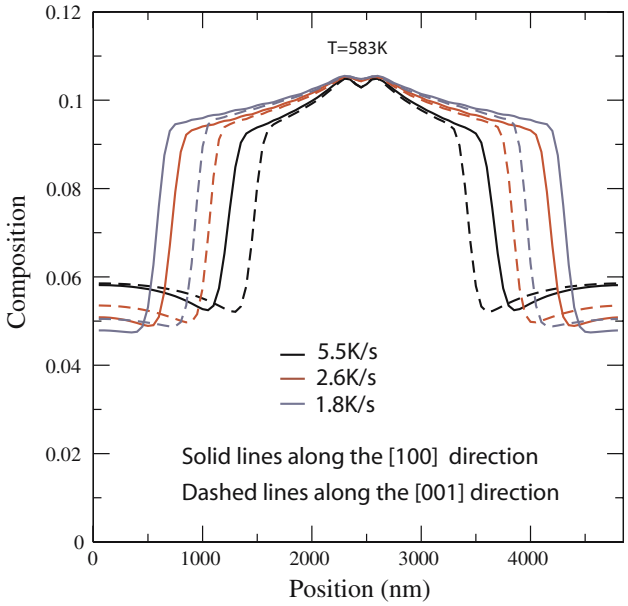

Fig. 10 Ga composition profile along a line through the center of the particle for different cooling rates 5.5 K/s, 2.6 K/s and 1.8 K/s at T = 583 K, respectively.

$$C_{ex} = \frac{1}{c_0 V_0} \int_V (c(\mathbf{r}, t) - c_0)\eta(\mathbf{r}, t) dV, \tag{26}$$

where V_0 is the volume of the system. The coring factor vs the volume faction of the fcc particle is plotted in Figure 11 for different cooling rates. It is clearly seen that the coring factor increases as the cooling rate decreases. This means that a slower cooling rate causes more Ga segregation in the fcc phase.

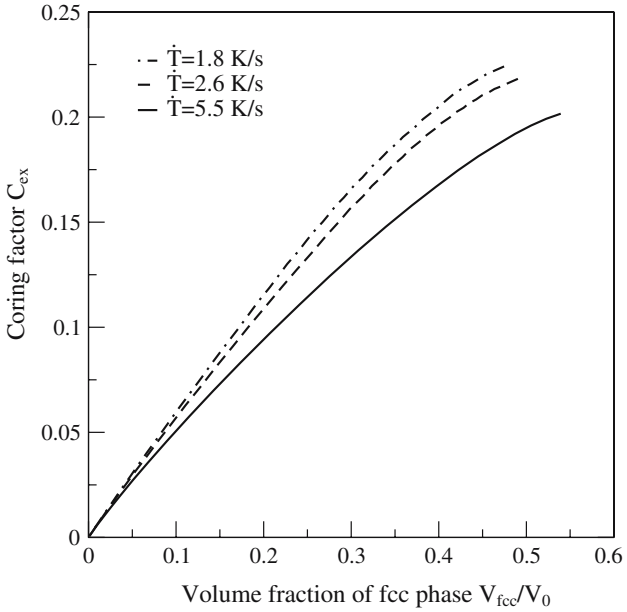

Fig. 11 Coring factor as a function of volume fraction of the fcc phase for different cooling rates.

Conclusion

A general phase-field model has been developed for simulating the coring structure evolution in Pu-Ga alloys. The model takes into account the strong inhomogeneity of Ga diffusivity and elastic properties, the elastic energy associated with the lattice mismatch, and the dependence of equilibrium compositions on the temperature. The simulations demonstrated that (1) the elastic energy associated with the lattice mismatch between the ε and δ phases results in the fastest growth in the $[100]_\varepsilon$ and $[010]_\varepsilon$ directions, and the slowest growth in the $[001]_\varepsilon$ direction, which leads to an elliptical particle. The aspect ratio of the elliptical particle increases with time. (2) the elastic inhomogeneity slows down the growth and increases the aspect ratio of the particle. (3) at constant temperature the effect of the inhomogeneity of Ga diffusivity on the growth is minor. (4) for a given fcc phase volume fraction the coring factor decreases as the cooling rate increases, i.e., the Ga segregation decreases as the cooling rate increases.

Acknowledgment

This work was supported at Los Alamos National Laboratory by the US Department of Energy under contract W-7405-ENG-36.

References

1. Zukas, E.G., Hecker, S.S., Morgan, J.R., Pereyra, R.A.: Solid-Solid Phase Transitions, pp. 1333 TMS-AIME, New York, NY (1982)
2. Hecker, S.S., Zukas, E.G., Morgan, J.R., Pereyra, R.A.: Solid-Solid Phase Transitions, pp. 1339 TMS-AIME, New York, NY (1982)

3. Ferrera, D.W., Doyle, H.J., Harvey, M.R.: RFP-1800, Rocky Flats Division, Dow Chemical USA, Golden, CO (1972)
4. Mitchell, J.N., Gibbs, F.E., Zocco, T.G., Pereyra, R.A.: Metal. Mater. Trans. A **32**, 649 (2001)
5. Zachariasen, W.H., Ellinger, F.H.: Acta Cryst., **16**, 780 (1963); Zachariasen, W.H., Ellinger, F.H.: Acta Cryst. **16**, 369 (1963); Zachariasen, W.H., Ellinger, F.H.: Acta Cryst. **8**, 431 (1955); and Ellinger, F.H.: AIME Trans. **206**, 1256 (1956)
6. Chen, L.Q.: Annu. Rev. Mater. Res. **32**, 113 (2002)
7. Karma, A., Rappel, W.: Phys. Rev. E **57**, 4323 (1998)
8. Li, Y.L., Hu, S.Y., Liu, Z.K., Chen, L.Q.: Appl. Phys. Lett. **81**, 427 (2002)
9. Wang, Y., Chen, L.Q., Khachaturyan, A.G.: Script. Metall. Et Mater. **25**, 1387 (1991)
10. Hu, S.Y., Chen, L.Q.: Acta Mater. **49**, 1879 (2001)
11. Hu S.Y., Baskes M.I., Stan S.M., Mitchell J.N.: Acta Mater., (submitted 2006).
12. Hecker, S.S.: Los Alamos Sci. **26**, 291 (2000)
13. Kim, S.G., Kim, W.T., Suzuki, T.: Phys. Rev. E **60**, 7186 (1999)
14. Hu, S.Y.: Phase-field Models of Microstructure Evolution in a System with Elastic Inhomogeneity and Defects, PhD Thesis, Department of Material Science & Engineering, The Pennsylvania State University (2004) http://etda.libraries.psu.edu/theses/approved/WorldWideIndex/ETD-478/
15. Miglioŗi A., Freibert, F., Lashley, J.C., Lawson, A.C., Baiardo, J.P., Miller, D.A.: J. Superconductivity: Incorporating Novel Magnetism **15**, 499 (2002)
16. Baskes, M.I., Hu, S.Y., Valone, S.M., Wang, G.F., Lawson, A.C.: (in preparation)
17. Zhang, J.X., Feng, W.M., Hu, S.Y., Liu, Z.K., Chen, L.Q.: (in preparation)
18. Cahn, J.W.: Acta Metall. **9**, 795 (1961)
19. Allen, S.M., Cahn, J.W.: Journal de Physique **38**, C7 (1977)
20. Edwards, G.R., Tate, R.E., Hakkila, E.A.: J. Nucl. Mater. **25**, 304 (1968)
21. Wade, W.Z.: J. Nucl. Mater. **38**, 292 (1971)
22. Chen, L.Q., Shen, J.: Comput. Phys. Comm. **108**, 147 (1998)